

Article

Assessing the Use of Burn Ratios and Red-Edge Spectral Indices for Detecting Fire Effects in the Greater Yellowstone Ecosystem

David M. Szpakowski ^{1,*}, Jennifer L. R. Jensen ², T. Edwin Chow ² and David R. Butler ²¹ Department of Earth and Environmental Science, Western Oregon University, Monmouth, OR 97361, USA² Department of Geography and Environmental Studies, Texas State University, San Marcos, TX 78666, USA; jjensen@txstate.edu (J.L.R.J.); chow@txstate.edu (T.E.C.); db25@txstate.edu (D.R.B.)

* Correspondence: szpakowskid@mail.wou.edu

† This manuscript is part of a Ph.D. thesis by the first author (David M. Szpakowski). Doctor program in Texas State University.

Abstract: Burn severity is commonly assessed using Burn Ratios and field measurements to provide land managers with estimates of the degree of burning in an area. However, less commonly studied is the ability of spectral indices and Burn Ratios to estimate field-measured fire effects. Past research has shown low correlations between fire effects and Landsat-derived Burn Ratios, but with the launch of the Sentinel-2 constellation, more spectral bands with finer spatial resolutions have become available. This paper explores the use of several red-edge-based indices and Burn Ratios alongside more ‘traditional’ spectral indices for predicting fire effects, measured from the Maple and Berry fires in Wyoming, USA. The fire effects include ash depth, char depth, post-fire dead lodgepole pine (*Pinus contorta*; PICO) density/stumps, mean basal diameter, cone density on dead post-fire trees, coarse wood percent cover/volume/mass, percent cover of ghost logs and initial regeneration of post-fire PICO/aspen density. All-possible-models regression was used to determine the best models for estimating each fire effect. Models with satisfactory R^2 values were constructed for post-fire dead PICO stumps (0.663), coarse wood percent cover (0.691), coarse wood volume (0.833), coarse wood mass (0.838), ash depth (0.636) and percent cover of ghost logs (0.717). Red-edge-based indices were included in all of the satisfactory models, which shows that the red-edge bands may be useful for measuring fire effects.

Keywords: fire; remote sensing; Burn Ratios; red-edge indices

Citation: Szpakowski, D.M.; Jensen, J.L.R.; Chow, T.E.; Butler, D.R. Assessing the Use of Burn Ratios and Red-Edge Spectral Indices for Detecting Fire Effects in the Greater Yellowstone Ecosystem. *Forests* **2023**, *14*, 1508. <https://doi.org/10.3390/f14071508>

Academic Editor: Viacheslav I. Kharuk

Received: 1 June 2023

Revised: 10 July 2023

Accepted: 17 July 2023

Published: 24 July 2023



Copyright: © 2023 by the authors. Licensee MDPI, Basel, Switzerland. This article is an open access article distributed under the terms and conditions of the Creative Commons Attribution (CC BY) license (<https://creativecommons.org/licenses/by/4.0/>).

1. Introduction

Burn severity is an important measurement of the effect that a wildfire has upon a landscape. Burn severity impacts vegetation mortality and soil nutrient composition, and causes increased runoff due to decreased infiltration resulting from soil hydrophobicity. The degree of burn severity can influence how long it takes for an ecosystem to recover and can change the composition of flora within an ecosystem. Because of these impacts, it is important for land managers to be able to assess the varying degrees of burn severity that result from fire events.

Burn severity can be measured differently depending on the interpretation of what it represents. Some studies have interpreted burn severity as a measurement of fire severity metrics and ecosystem responses [1]. Other researchers interpret burn severity solely as the loss of organic matter in the soil or on its surface. The latter approach is used for Burned Area Emergency Response (BAER) assessments, which commonly use the delta Normalized Burn Ratio (dNBR) to derive a burn severity map, designated as the Burned Area Reflectance Classification (BARC). BARC maps generally provide adequate assessments of post-fire vegetation conditions and allow for rapid assessment of the immediate impacts of a fire event [2]. BAER assessments commonly use the Composite Burn Index (CBI) for validation as it is heavily weighted towards the effects a fire has had on vegetation [3].

Although commonly used, the CBI possesses a major limitation because it is based on ocular measurements as opposed to more quantitative field methods [4]. This is because of how difficult it can be to take a significant number of accurate quantitative field measurements for each wildfire to calibrate spectral indices. However, this can lead to different assessments of CBI depending on the individual performing the assessment. Other measurements of burn severity provide a quantitative assessment of the level of burn severity, such as the amount of downed coarse wood, the number of live trees per unit area and ash depth.

The robustness of the dNBR Index has come into question, with several studies suggesting that the index does not always provide accurate estimates and needs improvement [5–7]. Miller and Thode [7] found that dNBR performs poorly for pixels containing sparse vegetation because of dNBR detecting absolute change. dNBR detects change through the use of the whole image, and so a large change relative to the land cover within a given pixel may not be considered a large change in the context of the image as a whole. Different vegetation compositions affected by the same fire and possessing the same degree of burning can be assigned dissimilar dNBR values. To address this issue, RdNBR was proposed.

RdNBR is designed to assess the relative change instead of absolute change. This is accomplished with an additional step to the dNBR procedure in which the square root of the absolute value of the pre-fire NBR is used to calculate the quotient of dNBR. Miller and Thode [7] found that RdNBR more accurately identified high-severity burns in areas of heterogeneous vegetation composition. However, the proposed equation possessed its own issues, namely, that the square root used to calculate RdNBR produces large, difficult-to-interpret numbers.

An alternative burn severity index was proposed by Parks et al. [8] and named the Relativized Burn Ratio (RBR). This index replaces the square root and absolute functions with the addition of 1.001 to ensure that all NBR values are greater than zero and altered in a way that preserves the level of NBR assigned to pixels. The RBR provides an index that estimates relative change without altering the output to the degree that the square-root in RdNBR does.

Although most studies using remote sensing data for assessing burn severity use Burn Ratios based on NIR and shortwave infrared (SWIR) [9], a proposed alternative to the Burn Ratios is to include land surface emissivity (LSE). The inclusion of LSE adds a surface characteristic that is separate from incoming solar radiation for the assessment of burn severity [10]. Quintano et al. [11] found that LSE-enhanced vegetation indices resulted in better burn severity estimates when compared to standard spectral indices, with an increase of about 16% when used to map burn severity in Sierra del Teleno, Spain. However, LSE-enhanced vegetation indices can be difficult to generate as they require the LSE and temperature to be differentiated from surface radiance and atmospheric conditions.

Spectral mixture analysis (SMA) has also been proposed as an alternative to Burn Ratios. SMA is a technique that uses the spectral reflectance of the ‘pure’ spectral response of land cover, referred to as endmembers, to determine the proportion of a mixed pixel belonging to different cover types. This is accomplished by using the endmembers to analyze a pixel and determine the degree to which the radiance from a mixed pixel agrees with each endmember [12]. Currently, SMA is not commonly used as a burn severity estimation technique. Studies that have compared spectral indices and SMA for estimating burn severity have shown the two approaches to be analogous [2,13]. However, SMA has not been shown to consistently outperform dNBR, as seen in Veraverbeke and Hook [13], which compared SMA to several spectral indices (NBR, dNBR, RdNBR) for burn severity estimates. They found that dNBR outperformed SMA but also noted that both approaches performed adequately and that SMA has the benefit of providing transferable quantitative data and does not need field data for calibration.

Recently, the Sentinel-2 sensor system was launched by the European Space Agency (ESA). The system contains additional red-edge bands that facilitate the calculation of more indices that may be useful for burn severity estimates. Fernández-Manso et al. [14] used

Sentinel-2 imagery to calculate several red-edge indices, as well as several more ‘traditional’ spectral indices, for estimating burn severity. They found that two of the red-edge indices outperformed the other indices that were tested, showing the potential for red-edge indices to aid in the assessment of burn severity. However, the capabilities of red-edge bands for assessing burn severity have not been fully explored and further research is needed.

Although most burn severity studies that use remote sensing to assess severity rely on field-measured CBI [5–7], few attempts have been published to determine which indices can be used for assessing more quantitative measurements of fire effects such as tree mortality by basal area and number of trees, char height and surface char. CBI is useful for the rapid ocular assessment of burn severity but is limited and may vary depending on the subjective judgement of the individual assessor in the field. Saberi [15] found that CBI estimates corresponded best to field measurements of tree canopy attributes but did not correspond as well to other field measurements like the deep char index. The authors suggest that spectral indices can be used to map CBI, which, in turn, can be used to map various fire effects (particularly those related to tree canopy attributes) using regression analysis. Hudak et al. [16] attempted to relate several Landsat 5 TM-derived burn indices to fire effects, finding that none of the indices were highly correlated with the fire effects.

The objective of this study is to test the ability of several indices to estimate field-measured fire effects using Sentinel-2 imagery. At present, the most commonly used burn indices, such as dNBR, RdNBR and RBR, are limited to broad near- and shortwave infrared band intervals. Limited research has been published that examines comparisons of red-edge bands to traditional data to calculate burn indices. In Fernández-Manso et al. [14], only post-fire indices were calculated, so this research aims to determine the effectiveness of using the delta index from pre- and post-fire imagery, as well as the post-fire indices. Additionally, alterations to the commonly used burn indices are made in which the narrow NIR band is replaced with a red-edge band to generate the indices and assess whether this substitution results in a more robust index.

By testing a broad range of indices, this paper seeks to determine the appropriate indices for estimating field-measured fire effects for two fires in the Greater Yellowstone Ecosystem. Given the limited availability of red-edge bands in free, publicly available data sets, this study contributes to an enhanced understanding of their utility for fire effects and associated estimates. Additionally, the findings from this study build on a limited body of knowledge regarding the specific effectiveness of Sentinel-2 red-edge bands for assessing post-fire effects. These bands are not present on similar publicly available sensors, such as Landsat 8 and 9.

2. Materials and Methods

2.1. Study Area

The Greater Yellowstone Ecosystem is located in northwestern Wyoming and includes Yellowstone National Park, Grand Teton National Park and their surrounding area (Figure 1). This study uses data collected from fires within Yellowstone National Park and Grand Teton National Park. Yellowstone National Park encompasses approximately 898,985 ha of land, including forests, mountains and glacial lakes. The northwestern portion of the park experienced the Maple Fire in the summer of 2016. The Maple Fire started on 8 August 2016 and burned until late October. The fire affected approximately 18,383 ha of land.

Grand Teton National Park encompasses approximately 130,000 ha of land that includes forests, mountains and glacial lakes. The northern section of Grand Teton National Park experienced a wildfire event in the late summer of 2016. The Berry Fire was discovered on 25 July 2016 and burned until early September of 2016. This fire affected approximately 8750 ha of land in and around the national park, causing the closure of Highway 89/191/287.

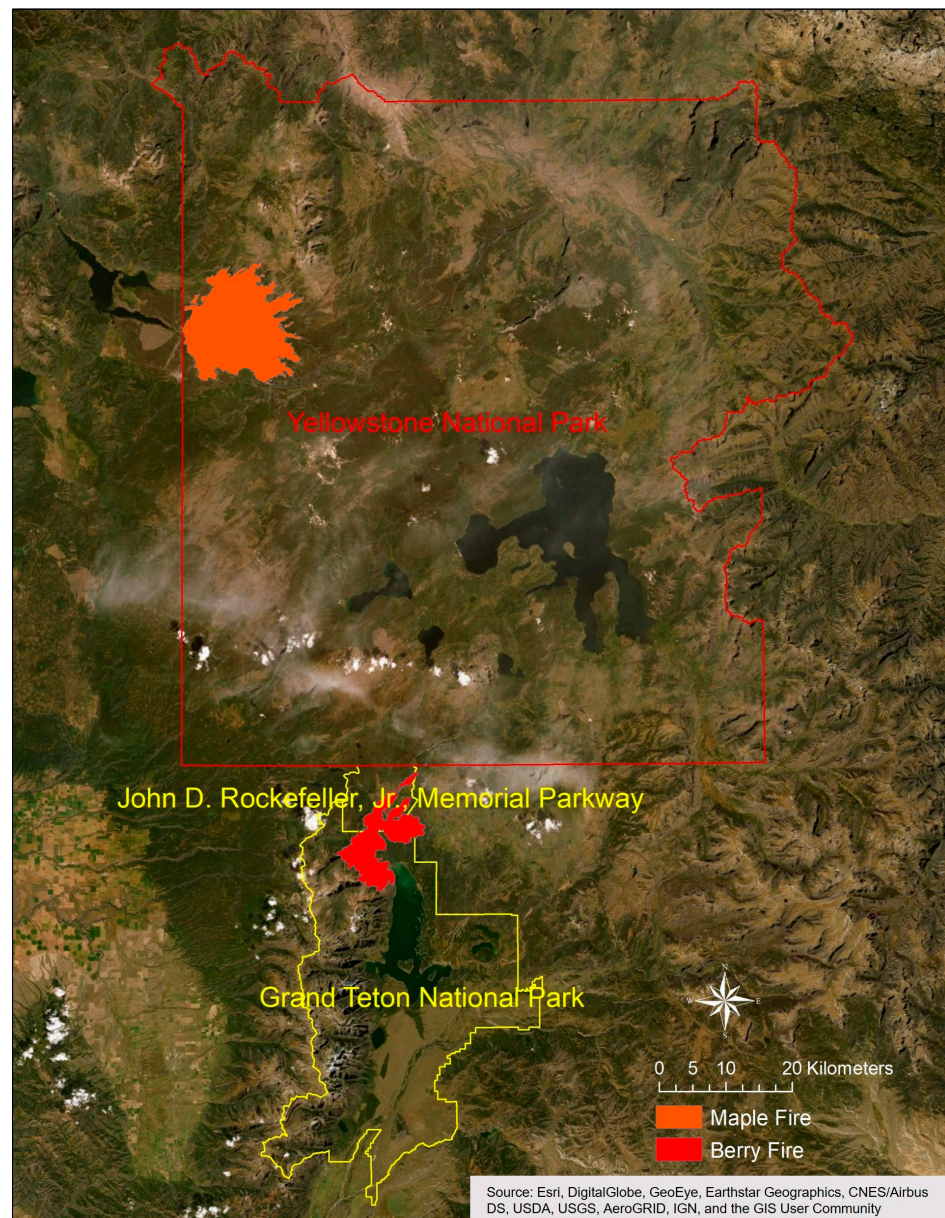


Figure 1. Study area within Greater Yellowstone Ecosystem, including Yellowstone National Park and Grand Teton National Park.

2.2. Field Data

The field data used in this research were collected by Turner et al. [17,18] in the summer of 2017. Turner et al. [17,18] collected several quantitative measurements for the Berry and Maple fires in the Greater Yellowstone Ecosystem to examine the effects of reburns on lodgepole pine (*Pinus contorta*; PICO) forests (Figure 2). Burn severity measurements for twenty-seven field plots were quantified using circular subplots measuring 30 m in diameter. The measurements collected within these plots included ash depth, char depth, post-fire dead PICO density/stumps, mean basal diameter, cone density on dead post-fire trees, coarse wood percent cover/volume/mass, percent cover of ghost logs and initial regeneration of post-fire PICO/aspen density (Table 1).

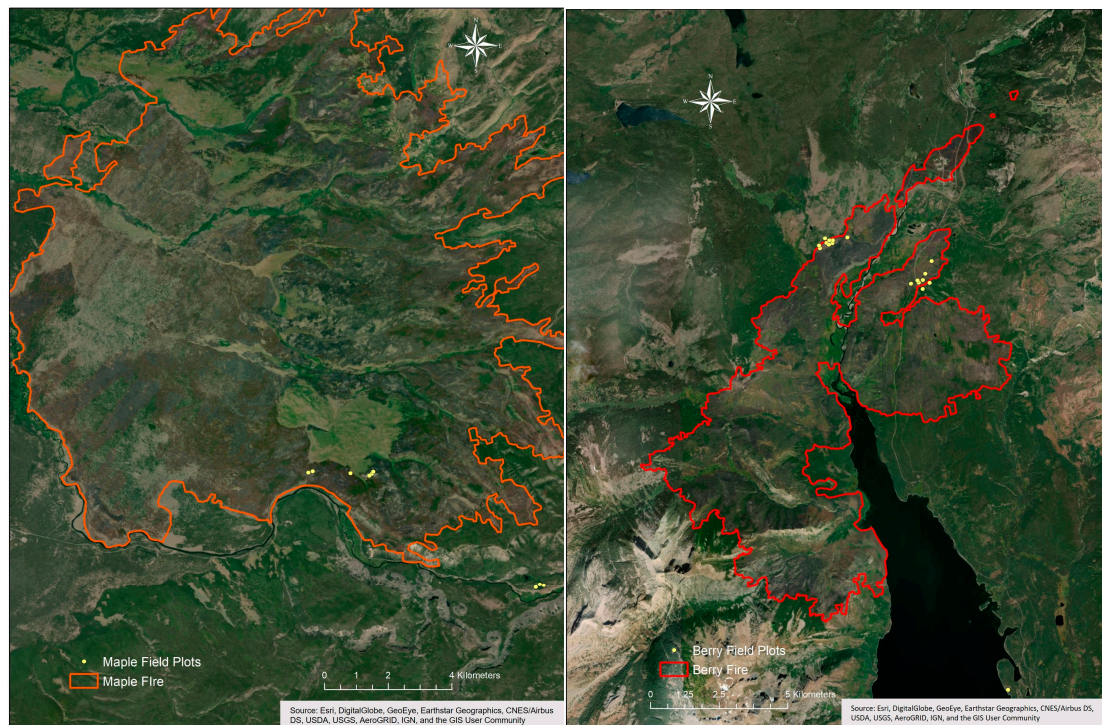


Figure 2. Locations of the twenty-seven field plots collected by Turner et al. [17] are shown as yellow points for the Maple (left) and Berry (right) fires.

Table 1. Field measurement definitions and units of measurement.

Field Measurement	Definition	Unit of Measurement
Post-fire Dead PICO Density	For plots that returned, the density of fire-killed lodgepole pine trees	Number per hectare
Post-Fire Dead PICO Stumps	For plots that returned, the density of stumps remaining for which the pre-fire lodgepole pine tree was completely combusted	Number per hectare
Mean Basal Diameter	The mean value from 25 measured live trees (on plots that did not return) or fire-killed trees or stumps (in returned plots)	Centimeters
Cone Density on Dead Post-fire Trees	In plots that returned, the remaining identifiable cones on fire-killed lodgepole pine trees	Number per hectare
Coarse Wood Percent Cover	Percent of surface covered by downed coarse wood, estimated via line intercept	Cubic meters per hectare
Coarse Wood Volume	Volume of coarse wood estimated via Brown's planar intercept transects; in returned plots, this is the volume of wood remaining after the short-interval fire	Megagrams per hectare
Coarse Wood Mass	Mass of coarse wood estimated via Brown's planar intercept transects; in returned plots, this is the volume of wood remaining after the short-interval fire	Millimeters

Table 1. Cont.

Field Measurement	Definition	Unit of Measurement
Ash Depth	Where recent ash was visible, depth on soil surface	Millimeters
Char Depth	If soil showed evidence of charring, depth from surface to which soil charring was evident	Millimeters
Percent Cover of Ghost Logs	On returned plots, areas of soil surface covered by log shadows where downed coarse wood had been combusted completely	Dimensionless
Initial Regeneration of Post-fire PICO Density	Density of first-year seedlings of lodgepole pine	Number per hectare
Initial Regeneration of Post-fire Aspen Density	Density of aspen stumps that resprouted from surviving roots; if multiple leaders came from the same stump, it was scored as one	Number per hectare

2.3. Image Preprocessing and Index Generation

Sentinel-2a data acquired on 15 July 2016 (pre-fire, Berry), 22 November 2016 (post-fire, Berry), 4 August 2016 (pre-fire, Maple) and 7 June 2017 (post-fire, Maple) were downloaded from the ESA open access data hub (<https://doi.org/10.6073/pasta/a1b7791376a04ce8c6ea9043547bb6af>, accessed on 12 May 2020) and from the USGS's EarthExplorer (<https://earthexplorer.usgs.gov/>, accessed on 30 March 2020). To ensure image pixel values were comparable, atmospheric corrections were performed using Sen2Cor to convert the data to surface reflectance. Two images were needed to capture the extent of the Maple fire for 4 August and 7 June, which were mosaiced together using nearest neighbor and most nadir seamline. For the Berry fire, the Monitoring Trends in Burn Severity's (MTBS) burned area shapefile was buffered by 6.5 km for use in this analysis, and for the Maple Fire, a 2 km buffer was applied to the MTBS burned area shapefile for analysis. These buffers were used to ensure that the collected control plots fell within the image data for analysis. The reason for the variation in buffer size is that the control plots for the Maple Fire were located within 2 km of the fire perimeter and the control plots for the Berry Fire were located within 6.5 km of the fire perimeter. The Berry and Maple fire images were then used to calculate several spectral indices (Table 1). Each of these indices was calculated for both the pre- and post-fire imagery, and then, the delta for each index were calculated by subtracting the post-fire image from the pre-fire image.

Additionally, RdNBR and RBR were calculated using the dNBR and NBR pre-fire (Equations (1) and (2)). These indices were calculated using the narrow NIR band (8a) to calculate dNBR, as shown in Table 2.

$$\text{RdNBR} = \frac{\text{dNBR}}{\sqrt{|\text{NBR}_{\text{pre-fire}}|}} \quad (1)$$

where dNBR was calculated using the difference between pre- and post-fire NBR.

$$\text{RBR} = \frac{\text{dNBR}}{\text{NBR}_{\text{pre-fire}} + 1.001} \quad (2)$$

Table 2. List of indices generated for estimating burn severity.

Spectral Indices	Column 2	Equation
NBR	Normalized Burn Ratio	$\frac{B8a - B12}{B8a + B12}$
NDVI	Normalized Difference Vegetation Index	$\frac{B8a - B4}{B8a + B4}$
GNDVI	Green Normalized Difference Vegetation Index	$\frac{B8a - B3}{B8a + B3}$
NDVIre1n	Normalized Difference Vegetation Index red-edge 1 narrow	$\frac{B8a - B5}{B8a + B5}$
NDVIre2n	Normalized Difference Vegetation Index red-edge 2 narrow	$\frac{B8a - B6}{B8a + B6}$
NDVIre3n	Normalized Difference Vegetation Index red-edge 3 narrow	$\frac{B8a - B7}{B8a + B7}$
PSRI	Plant Senescence Reflectance Index	$\frac{B4 - B3}{B6}$
Clre	Chlorophyll Index re-edge	$\frac{B7}{B1} - 1$
Ndre1	Normalized Difference re-edge 1	$\frac{B6 - B5}{B6 + B5}$
Ndre2	Normalized Difference re-edge 2	$\frac{B7 - B5}{B7 + B5}$
MSRren	Modified Simple Ratio red-edge narrow	$\frac{\left(\frac{B8a}{B5}\right) - 1}{\sqrt{(B8a/B5) + 1}}$

Further, alternative red-edge-based dNBRs, RdNBRs and RBRs were generated (three each) by replacing the narrow NIR band (0.8483–0.8813 μm) with Sentinel-2 bands five (0.6955–0.7134 μm), six (0.7312–0.7492 μm) and seven (0.7685–0.7965 μm). This was carried out to determine how accurately red-edge versions of dNBR, RdNBR and RBR estimated the various burn severity metrics. The red-edge is a region within the electromagnetic spectrum from 0.680 to 0.750 μm . The spectral response curve for healthy vegetation with high chlorophyll content will display a sharp increase in spectral reflectance in this region [19]. In the past, the lack of freely available red-edge remote sensing data made it difficult to explore the potential for these wavelengths to enhance burn severity assessment. The resulting dNBR indices for the Berry Fire study area can be seen in Figure 3.

2.4. Analysis

The x , y locations for each field data point were entered into a GIS environment with the recorded field measurements as attributes. Next, a 30 m buffer was applied to each plot point and zonal statistics were calculated to determine the mean value of pixels that fell within the buffer. This was carried out because the field plots collected by Turner et al. [17,18] were collected in 30 m circular plots, and so will encompass multiple 20 m Sentinel-2 pixels. By buffering and using zonal statistics, the mean of these pixels can be extracted and this value will better correspond to the field measurements than using just the value of the pixel that plot centers fell into. Finally, the mean values for each index were extracted to these points. A correlation matrix was generated to determine whether a relationship between the field measurements and the spectral indices exists. Finally, using all-possible-models regression, models for predicting the field-measured burn severity metrics using the spectral indices were constructed. These models were validated using the prediction error sum of squares (PRESS) statistic, a form of leave-one-out cross-validation.

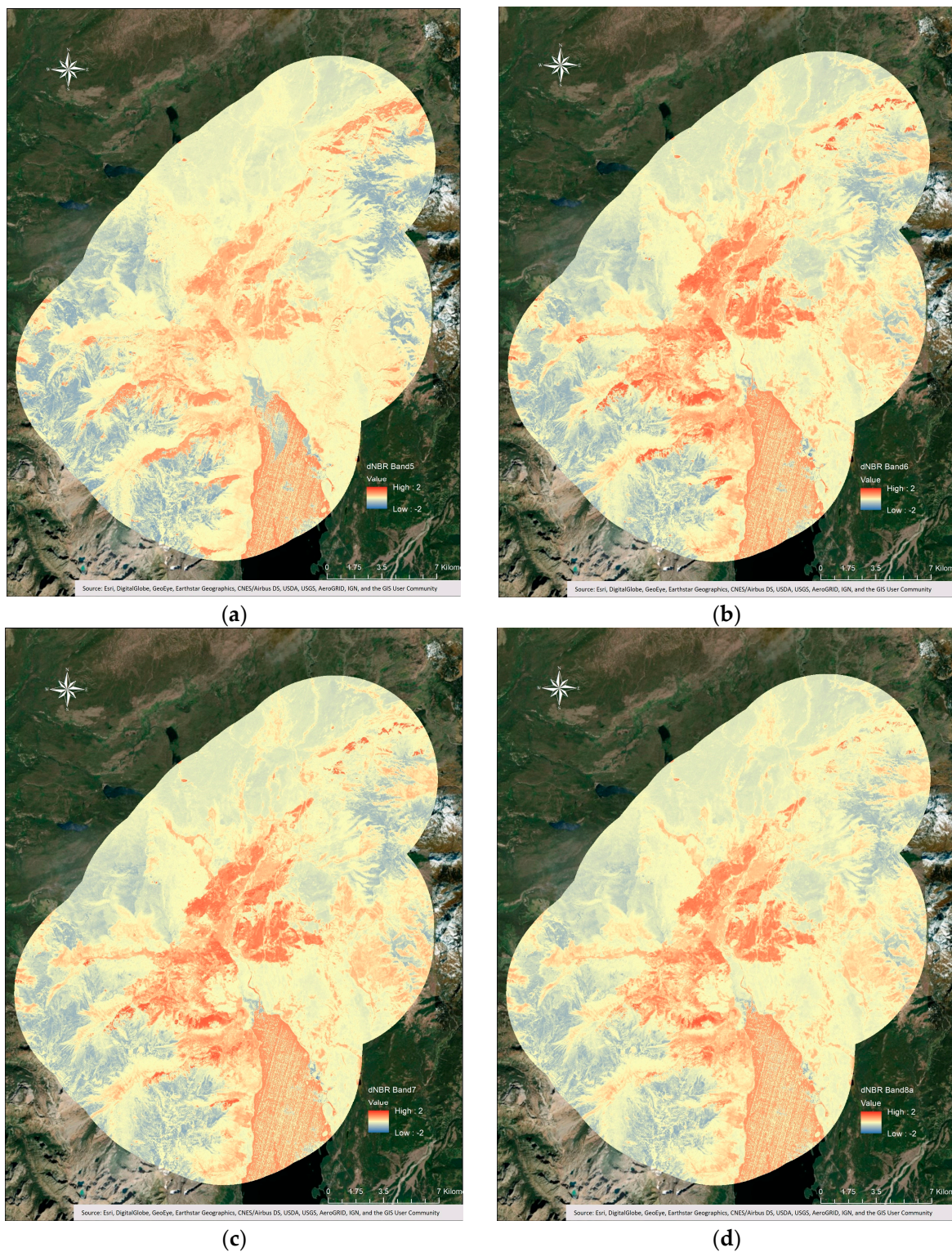


Figure 3. The dNBR index, calculated using bands five (0.6955–0.7134 μm) (a), six (0.7312–0.7492 μm) (b), seven (0.7685–0.7965 μm) (c) and eight-a (0.8483–0.8813 μm) (d). The symbology is stretched to a range of -2 to 2 so the indices can be more easily compared.

3. Results

3.1. Descriptive Statistics for Spectral Indices

The spectral indices were generated for a 6.5 km buffered area around the Berry Fire and for the 2 km buffered area of the Maple Fire. Table 3 shows the descriptive statistics

for each spectral index calculated for the Berry Fire grouped into five categories: post-fire normalized red-edge indices, difference normalized red-edge indices, difference normalized Burn Ratios, other Burn Ratios and other indices ($n = 1,478,229$ pixels). The non-Burn Ratio indices are defined in Table 2. In Table 3 the PF following the index acronym signifies post-fire, while the d before the index acronym signifies the result of the delta between pre- and post-fire imagery. For the Burn Ratios, the B# following the index signifies which red-edge band was used for NIR in the NBR equation. Table 4 shows the same breakdown of indices for the Maple Fire ($n = 970,055$ pixels). Note that the CLre, MSRren and PSRI indices are also red-edge indices, which are not normalized, and so are grouped under other indices, whereas the GNDVI indices are normalized but are not red-edge indices and so are also under other indices.

Table 3. Descriptive statistics for Berry Fire indices.

Index	Min	Max	Mean	Standard Deviation
Post-fire Normalized Red-edge Indices				
NDre1_PF	−0.994	0.997	0.130	0.222
NDre2_PF	−0.994	0.998	0.154	0.244
NDVIre1n_PF	−0.996	0.998	0.178	0.264
NDVIre2n_PF	−0.986	0.993	0.060	0.109
NDVIre3n_PF	−0.987	0.992	0.031	0.078
Difference Normalized Red-edge Indices				
dNDre1	−1.202	1.805	0.025	0.152
dNDre2	−1.719	1.946	0.026	0.151
dNDVIre1n	−1.857	1.892	0.017	0.145
dNDVIre2n	−1.747	1.787	−0.011	0.094
dNDVIre3n	−1.886	1.798	−0.013	0.078
Difference Normalized Burn Ratios				
dNBR_B8a	−1.749	1.637	0.010	0.423
dNBR_B5	−1.798	1.666	−0.036	0.436
dNBR_B6	−1.769	1.627	0.026	0.479
dNBR_B7	−1.736	1.693	0.030	0.460
Other Burn Ratios				
RdNBR_B8a	−73.309	32.330	−0.133	1.612
RdNBR_B5	−84.548	42.966	−0.318	2.002
RdNBR_B6	−68.660	48.944	−0.214	1.937
RdNBR_B7	−75.090	28.094	−0.148	1.765
RBR_B8a	−70.076	0.994	−0.014	0.442
RBR_B5	−198.320	0.996	−0.073	0.609
RBR_B6	−161.290	0.997	−0.021	0.657
RBR_B7	−159.930	0.997	−0.007	0.534
Other Indices				
GNDVI_PF	−0.997	0.999	0.270	0.436
PSRI_PF	−280.000	80.000	−2.107	17.112
MSRren_PF	−0.997	28.284	0.466	1.194
CLre_PF	−3836.000	3662.000	217.252	365.007
dGNDVI	−1.627	1.624	0.012	0.205
dPSRI	−295.300	279.860	1.944	17.172
dMSRren	−27.486	15.185	−0.081	1.048
dCLre	−2740.000	4979.000	297.265	523.168

3.2. Correlation Results

To determine whether the indices and field measurements were related, Pearson correlations between the field measurement and spectral indices were assessed (Table 5; $n = 27$). Coarse wood percent cover and coarse wood mass were correlated with the most indices, with each field measurement possessing strong correlations with twenty-two spectral indices. Other field measurements that possessed strong correlations with spectral indices

were post-fire dead PICO stumps, ash depth, coarse wood volume and percent cover of ghost logs.

Table 4. Descriptive statistics for Maple Fire indices.

Index	Min	Max	Mean	Standard Deviation
Post-fire Normalized Red-edge Indices				
NDre1_PF	−0.829	0.947	0.168	0.138
NDre2_PF	−0.991	0.967	0.204	0.155
NDVire1n_PF	−0.990	0.941	0.238	0.165
NDVire2n_PF	−0.981	0.882	0.077	0.047
NDVire3n_PF	−0.974	0.994	0.037	0.027
Difference Normalized Red-edge Indices				
dNDre1	−0.912	0.708	0.049	0.123
dNDre2	−0.867	0.735	0.057	0.128
dNDVire1n	−0.828	0.893	0.059	0.117
dNDVire2n	−1.172	0.997	0.015	0.022
dNDVire3n	−1.022	0.762	0.005	0.020
Difference Normalized Burn Ratios				
dNBR_B8a	−0.888	1.229	0.159	0.294
dNBR_B5	−1.207	0.938	0.072	0.181
dNBR_B6	−1.028	1.260	0.140	0.301
dNBR_B7	−0.969	1.268	0.154	0.306
Other Burn Ratios				
RdNBR_B8a	−59.367	18.309	0.248	0.652
RdNBR_B5	−15.804	23.850	0.352	1.120
RdNBR_B6	−45.937	26.669	0.275	0.994
RdNBR_B7	−56.675	23.814	0.257	0.827
RBR_B8a	−7.268	0.985	0.114	0.214
RBR_B5	−1.747	0.983	0.076	0.196
RBR_B6	−69.379	0.852	0.106	0.259
RBR_B7	−53.673	0.989	0.112	0.243
Other Indices				
GNDVI_PF	−0.985	0.995	0.409	0.250
PSRI_PF	−9.818	1.238	0.053	0.087
MSRren_PF	−0.993	5.488	0.423	0.319
CLre_PF	−1447.000	4516.000	556.645	540.477
dGNDVI	−0.717	1.349	0.058	0.113
dPSRI	−1.211	13.981	−0.014	0.097
dMSRren	−5.318	1.423	0.130	0.262
dCLre	−1447.000	13.981	−0.014	0.097

Coarse wood mass possessed the strongest positive relationship with the spectral index, with NDre2_PF having a correlation of 0.886. The NDre2_PF index also possessed a strong positive correlation with coarse wood percent cover and coarse wood volume. Coarse wood mass also possessed the strongest negative correlation of −0.811 with both dNDre2 and GNDVI_PF.

dNDre2_PF was significantly related to the most field measurements, with six field-measured fire effects being strongly correlated with this index. The RdNBR_B8a index was significantly correlated with only one field measurement, coarse wood percent cover. Several indices were found not to possess strong correlations with any field measurements, including dPSRI, dNDVire2n, dNDVire3n, NDVire2n_PF, NDVire3n_PF and RdNBR_B5.

Table 5. Correlations between field measurements and spectral indices. Strong positive correlations ($r \geq 0.60$) are highlighted in green and strong negative correlations ($r \leq -0.60$) are highlighted in orange.

Index	Post-fire Dead PICO Density	Post-fire Dead PICO Stumps	Mean Basal Diameter	Post-fire Cone Density	Coarse Wood Percent	Coarse Wood Volume	Coarse Wood Mass	Ash Depth	Char Depth	Percent Cover of Ghost Logs	Initial Regen PICO	Initial Regen Aspen
dCLre_Avg	0.294	0.358	-0.167	0.443	-0.669	-0.551	-0.617	0.674	0.227	0.518	0.274	0.346
dPSRI_Avg	-0.170	-0.078	0.001	-0.295	0.529	0.367	0.438	-0.515	-0.440	-0.387	-0.038	-0.328
MSRren_AVG	0.283	0.636	-0.417	0.345	-0.636	-0.754	-0.742	0.572	-0.195	0.491	0.484	0.094
NDre1_Avg	0.352	0.565	-0.354	0.462	-0.756	-0.765	-0.798	0.696	0.088	0.581	0.414	0.190
NDre2_AVG	0.346	0.658	-0.428	0.418	-0.752	-0.793	-0.811	0.697	-0.021	0.580	0.450	0.139
NDVire1n_A	0.291	0.726	-0.481	0.291	-0.657	-0.777	-0.763	0.626	-0.160	0.552	0.460	0.065
NDVire2n_A	-0.139	0.228	-0.183	-0.326	0.243	0.037	0.126	-0.194	-0.477	-0.111	0.070	-0.240
NDVire3n_A	-0.040	0.344	-0.537	-0.172	-0.057	-0.430	-0.354	0.107	-0.315	0.201	0.131	-0.005
CLre_PF_Avg	-0.316	-0.347	0.204	-0.379	0.671	0.587	0.658	-0.673	-0.281	-0.587	-0.260	-0.286
PSRI_PF_AVG	0.142	0.018	0.034	0.263	-0.499	-0.337	-0.413	0.469	0.472	0.371	0.001	0.318
MSR_PF_AVG	-0.145	-0.623	0.524	-0.026	0.650	0.808	0.776	-0.485	0.185	-0.580	-0.331	-0.120
NDre1_PF_AVG	-0.258	-0.557	0.431	-0.257	0.821	0.855	0.883	-0.668	-0.139	-0.688	-0.312	-0.212
NDre2_PF_AVG	-0.235	-0.658	0.522	-0.174	0.805	0.879	0.886	-0.649	0.001	-0.686	-0.337	-0.162
NDVire1_PF_A	-0.167	-0.707	0.570	-0.022	0.671	0.826	0.798	-0.548	0.153	-0.630	-0.330	-0.085
NDVire2_PF_A	0.133	-0.280	0.259	0.367	-0.172	0.035	-0.059	0.153	0.485	0.038	-0.062	0.181
NDVire3_PF_AVG	0.168	-0.162	0.147	0.375	-0.260	-0.042	-0.137	0.230	0.431	0.089	-0.020	0.161
dNBR_B5_AVG	0.415	0.326	-0.277	0.551	-0.612	-0.569	-0.641	0.667	0.290	0.443	0.372	0.195
dNBR_B6_AVG	0.418	0.358	-0.299	0.539	-0.626	-0.589	-0.656	0.683	0.238	0.477	0.359	0.230
dNBR_B7_AVG	0.412	0.385	-0.293	0.549	-0.641	-0.600	-0.667	0.687	0.266	0.484	0.380	0.197
dNBR_8a_AVG	0.417	0.414	-0.319	0.547	-0.644	-0.619	-0.682	0.703	0.257	0.499	0.397	0.190
RBR_B5_AVG	0.388	0.272	-0.249	0.519	-0.610	-0.552	-0.626	0.650	0.333	0.463	0.325	0.346
RBR_B6_AVG	0.382	0.334	-0.278	0.501	-0.658	-0.603	-0.671	0.678	0.314	0.520	0.274	-0.328
RBR_B7_AVG	0.387	0.356	-0.294	0.501	-0.660	-0.608	-0.675	0.688	0.306	0.518	-0.038	0.094
RBR_8a_AVG	0.396	0.390	-0.322	0.503	-0.663	-0.630	-0.693	0.706	0.293	-0.387	0.484	0.190
RdNBR_B5_AVG	0.383	0.326	-0.180	0.520	-0.425	-0.414	-0.479	0.468	0.227	0.491	0.414	0.139
RdNBR_B6_AVG	0.208	0.172	-0.253	0.273	-0.615	-0.554	-0.614	0.674	-0.440	0.581	0.450	0.065
RdNBR_B7_AVG	0.228	0.205	-0.250	0.296	-0.673	-0.584	-0.617	-0.515	-0.195	0.580	0.460	-0.240
RdNBR_8a_AVG	0.353	0.349	-0.325	0.441	-0.687	-0.551	0.438	0.572	0.088	0.552	0.070	-0.005
GNDVI_AVG	0.237	0.709	-0.541	0.124	-0.669	0.367	-0.742	0.696	-0.021	-0.111	0.131	-0.286
NDVI_AVG	0.357	0.705	-0.479	0.443	0.529	-0.754	-0.798	0.697	-0.160	0.201	-0.260	0.318
GNDVI_PF_AVG	-0.131	-0.673	-0.167	-0.295	-0.636	-0.765	-0.811	0.626	-0.477	-0.587	0.001	-0.120

3.3. Regression Results

Within the statistical analysis software JMP 14, all-possible-models (i.e., best subsets regression) was used to construct models for predicting field measurements using the spectral indices. All-possible-models regression tests all possible subsets of the predictor variables, and returns models that contain one variable, two variables, etc., along with their summary statistics. This allows the researcher to quickly assess the performance of every combination of predictor variables to determine which models performed best. With a sample size of twenty-seven field plots, a maximum of three independent variables were allowed for model construction. Each model was assessed based on the significance of its independent variables and on the variable multicollinearity. The p -value of each model covariate had to be less than 0.05 for the model to be accepted. Multicollinearity was assessed using the Variance Inflation Factor (VIF), where all input variables had to possess VIF values of < 10 . The models for one, two and three input variables that met these criteria and possessed the highest R^2 for a given field measurement are reported in Table 6.

Table 6. Results from all-possible-models regression. Models with moderately strong results ($0.6 < R^2 < 0.7$) are highlighted in yellow, while models with $R^2 > 0.7$ are highlighted in green.

Field Measurement	Model Variables	R^2	RMSE	PRESS R^2	PRESS RMSE
Post-fire Dead PICO Density	dNBR_B6	0.174	16,859.88	0.066	17,255.543
Post-fire Dead PICO Density	None	N/A	N/A	N/A	N/A
Post-fire Dead PICO Density	None	N/A	N/A	N/A	N/A
Post-fire Dead PICO Stumps	dNDVIre1n	0.527	21,687.91	0.383	23,854.682
Post-fire Dead PICO Stumps	dNBR_B5, dNDVI	0.663	18,705.19	0.502	21,414.479
Post-fire Dead PICO Stumps	None	N/A	N/A	N/A	N/A
Mean Basal Diameter	GNDVI_Pf	0.349	2.542	0.248	2.629
Mean Basal Diameter	dNDVIre3n, NDre2_Pf	0.440	2.406	0.2853	2.562
Mean Basal Diameter	None	N/A	N/A	N/A	N/A
Cone Density on Dead Post-fire Trees	dNBR_B5	0.304	75,553.4	0.184	78,703.305
Cone Density on Dead Post-fire Trees	dNDre2, NDVIre1n_Pf	0.419	70,417.16	0.2411	75,900.966
Cone Density on Dead Post-fire Trees	dPSRI, dMSRren, NDVIre2n_Pf	0.571	61,865.44	0.333	71,184.947
Coarse Wood Percent Cover	NDre1_Pf	0.674	3.244	0.620	3.370
Coarse Wood Percent Cover	MSRren_Pf, dNDVIre3n	0.691	3.226	0.627	3.341
Coarse Wood Percent Cover	None	N/A	N/A	N/A	N/A
Coarse Wood Volume	NDre2_Pf	0.773	42.735	0.7403	43.944
Coarse Wood Volume	dNDVIre3n, NDre1_Pf	0.833	37.336	0.782	40.229
Coarse Wood Volume	None	N/A	N/A	N/A	N/A
Coarse Wood Mass	NDre2_Pf	0.784	15.878	0.753	16.367
Coarse Wood Mass	dNDVIre3n, NDre1_Pf	0.838	14.066	0.787	15.175
Coarse Wood Mass	dNDVIre3n, NDre2_Pf, NDVIre2n_Pf	0.842	14.157	0.770	15.776
Ash Depth	dNDVI	0.548	3.455	0.493	3.520
Ash Depth	dCLre, dNDVIre3n	0.581	3.396	0.486	3.543

Table 6. Cont.

Field Measurement	Model Variables	R ²	RMSE	PRESS R ²	PRESS RMSE
Ash Depth	dPSRI, dNDVIre2n, dNBR_B5	0.636	3.233	0.392	3.853
Char Depth	NDVIre2n_PF	0.235	0.177	−0.008	0.195
Char Depth	dNDre2, RBR_B8a	0.328	0.169	0.148	0.179
Char Depth	None	N/A	N/A	N/A	N/A
Percent Cover of Ghost Logs	NDre1_PF	0.473	2.430	0.361	2.574
Percent Cover of Ghost Logs	NDVIre1n_PF, RdNBR_B5	0.587	2.194	0.421	2.450
Percent Cover of Ghost Logs	dNDre2, NDVIre1n_PF, RdNBR_B5	0.717	1.855	0.574	2.100
Initial Regeneration of Post-fire PICO Density	dMSRren	0.234	8440.969	0.030	9140.458
Initial Regeneration of Post-fire PICO Density	RBR_B6, PSRI_PF	0.328	8071.69	0.078	8915.812
Initial Regeneration of Post-fire PICO Density	None	N/A	N/A	N/A	N/A
Initial Regeneration of Post-fire Aspen Density	None	N/A	N/A	N/A	N/A
Initial Regeneration of Post-fire Aspen Density	MSRren_PF, GNDVI_PF	0.249	81.299	0.037	86.791
Initial Regeneration of Post-fire Aspen Density	dCLre, dNDVIer3n, dNDVI	0.448	71.177	0.224	77.933

Of the field measurements, coarse post-fire dead PICO stumps, coarse wood percent cover, coarse wood volume, coarse wood mass, ash depth and percent cover of ghost logs possessed models with R²s above 0.6. Of these, coarse wood mass achieved the highest R² (0.847), followed by Coarse wood volume (R² = 0.833). Ash depth had the lowest R² (0.636), with post-fire dead PICO stumps possessing the second lowest (R² = 0.663) of the variables with R²s greater than 0.6.

Of the single-variable models, Coarse wood volume possessed the highest R² (0.784) with NDre2_PF as the input variable. The single-variable model for post-fire dead PICO density performed the worst, with an R² of 0.174 when dNBR_B6 was used as the input variable. For the two-variable models, coarse wood mass performed the best, with an R² of 0.847, and initial regeneration of post-fire aspen density performed the worst, with an R² of 0.249. Of the three-variable models, coarse wood mass possessed the highest R² (0.847), whereas initial regeneration of post-fire aspen density had the lowest R² (0.448). Several field measurements did not have any models that met the *p*-value and/or VIF criteria, and so their variables are reported as none and their statistics as N/A.

The PRESS statistic was used to determine which of the models generated for each field measurement possessed the best predictive power. This statistic determines model performance by leaving one sample out at a time to determine how well the data predict the left-out sample [20]. The model with an R² > 0.60 that yielded the highest PRESS R² for each field measurement was determined to be the best model for predicting the field-measured fire effect. Standard least squares was then used to plot these models and determine their corresponding prediction equation (Figure 4).

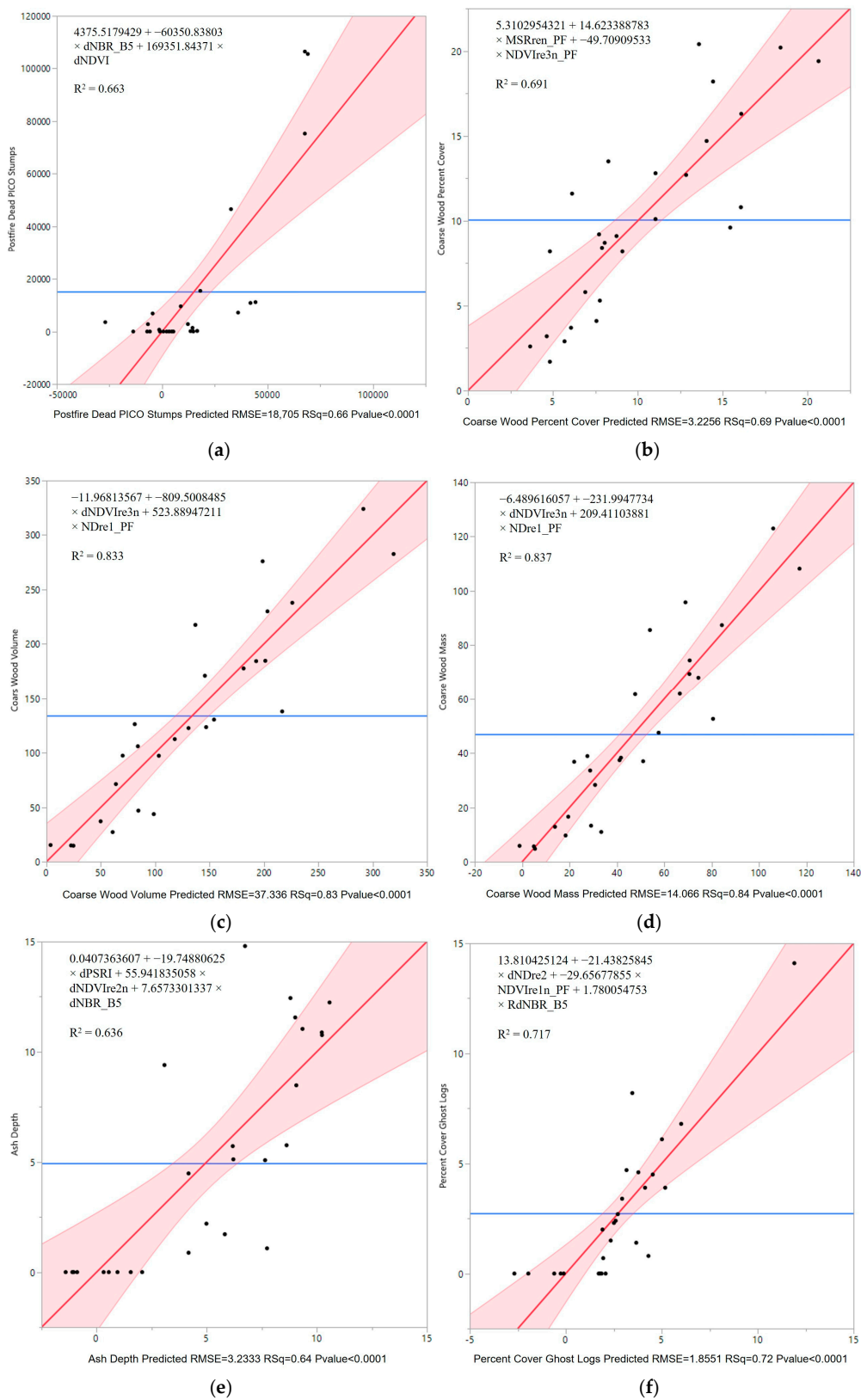


Figure 4. Standard Least Squares for models with best predictive capabilities for post-fire dead PICO stumps (a), coarse wood percent cover (b), coarse wood volume (c), coarse wood mass (d), ash depth (e) and percent cover of ghost logs (f). The red line is the line of fit, the blue line is the mean line and the red buffer zone is the confidence interval.

Of the variables used to construct these models, dNDVIre3n, NDre1_PF and dNBR_B5 were the only indices used in more than one model. A total of three Burn Ratio indices were used across all the models, whereas ten red-edge indices were used. Of the Burn Ratio indices, all the selected input variables for the models used red-edge bands in place of narrow NIR.

4. Discussion

4.1. Correlations between Spectral Indices and Field Measurements

When examining the correlation between the various spectral indices and the fire effects measurements, the strongest correlations were found to involve indices generated using band 5 for all field measurements. Of the red-edge indices, the only indices to possess strong correlations with field measurements not generated using band 5 were CLre_PF and dCLre. Of the red-edge NDVI indices, both post-fire and difference NDVIre1n outperformed their NDVIre2n and NDVIre3n counterparts. Previous research has reported similar findings, with red-edge indices generated using the band closest to red, band 5, outperforming the other red-edge indices, as well as more traditional spectral indices, for burn severity detection [14,21].

4.2. Spectral Indices' Ability to Estimate Field Measurements

Although many studies have estimated burn severity using spectral indices [5–7], only a few have attempted to estimate field-measured fire effects using these indices [16,22,23]. Although field-measured fire effects are not as commonly assessed because of the time-intensive nature of these measurements, they provide valuable ecological information that can be used in fire recovery efforts. However, previous research has shown little relationship between Landsat-derived burn indices and field-measured fire effects [16,22,23]. This can be attributed to a number of variables, including the spatial resolution of Landsat images, the radiometric resolution of the sensors used during the time of these studies being inadequate to capture the slight variations in radiance, and the lack of spectral bands in the red-edge region. Previous research has shown slight improvement in the performance of Sentinel-2 NBR-based indices when compared to Landsat 8 NBR-based indices [24,25]. However, this research was limited to indices that could be calculated by both sensor systems, which eliminates the use of red-edge indices. The results of this research suggest that several field-measured fire effects can be estimated using the Sentinel-2 sensor constellation, and the use of red-edge indices improved Sentinel-2's performance of this task.

Of the fire effects estimated by the spectral indices, those related to tree canopy characteristics resulted in the best estimates. This agrees with the findings of Saberi [15], who found that CBI and the three primary burn severity indices (dNBR, RdNBR, and RBR) were more highly correlated with tree canopy fire effects than they were with other effects. Additionally, we found that the red-edge spectral indices explained approximately 64% of field-measured variation in ash depth and 72% of the variation in percent cover of ghost logs.

Of the best-performing models, coarse wood mass and coarse wood volume possessed the highest R^2 values, at 0.837 and 0.833, respectively. Both models were generated using the same red-edge indices, with neither of the models requiring a Burn Ratio index. These high accuracies, combined with the use of solely red-edge indices, suggest that further research into the utility of using red-edge indices for estimating and mapping various fire effects should be explored.

4.3. Performance of Red-Edge Bands and Indices

With the launch of the Sentinel-2 sensor constellation, red-edge bands for index generation have become freely available. Fernández-Manso et al. [14] show that red-edge indices can accurately discriminate between levels of burn severity and found that indices generated using Sentinel-2 band five were most suited to this task. Our results show that

indices that were generated using band five were included in all six of the best-performing models, suggesting agreement with other research [14,21,26].

Interestingly, of the best-performing models, only one contained a non-red-edge index (percent dead PICO stumps). The two best-performing models (coarse wood volume and mass) both only used red-edge indices, and both achieved $R^2 > 0.8$. The indices used in these models relied on bands 5, 7 and 8a. This suggests that red-edge indices, which have shown promising results in estimating burn severity [14,21,27], may also be useful for estimating fire effects.

4.4. Sources of Uncertainty

Although these results are promising, there are a few sources of uncertainty. The largest sources of uncertainty are the sample size of the field data ($n = 27$) as well as the limitation of the data to a single ecosystem. As a result, the data do not provide a comprehensive explanation for the tested dependent variables, and our results should be considered preliminary.

The field measurements were collected for circular subplots measuring 30 m in diameter, but the spatial resolution of the Sentinel-2 data was 20 m. We used the average of the pixels that fell within a 30 m buffer to address this issue, but some of these pixels lay partially outside the buffer and other pixels were excluded because too small a proportion of these pixels fell within the buffer. This may lead to the spectral reflectance of the pixels corresponding to these measurements only partially representing the measured conditions and/or including reflectance from outside the buffer in the average.

Additionally, a geolocation error between images can create uncertainty in index calculation and value-to-points extraction. For Sentinel-2, this error is less than 1 pixel in most cases, with errors exceeding this threshold primarily because of coarse corrections. No coarse corrections were documented for any of the images used in this analysis; however, a single pixel error could potentially impact the results.

The use of samples from two separate fires is also a source of uncertainty. These fires started and ended around the same time (summer 2016 to fall 2016) and were both located in the Greater Yellowstone Ecosystem, possessing similar vegetation and landcover. However, different image acquisition dates and a more limited number of samples for the Maple Fire could create uncertainty in the results. However, because of the lack of snow cover in the November imagery and the evergreen forests that make up the majority of the in-scene vegetation for both fires, we do not expect the difference in acquisition dates to considerably influence our results. After examining the residuals for the primary regression models, it was noted that overall, the two fires' residuals were similarly distributed, except in the case of post-fire dead PICO stumps, where the upper end of the predicted values for the Maple Fire possessed larger negative and positive residuals than any residual for the Berry Fire. This can be explained by the limited sampling for both fires, which ideally would have at least thirty sample plots per fire. Because of this limited sample size, these results should be considered preliminary and further research should be conducted to determine their validity.

5. Conclusions

This study assessed the ability of spectral indices, both traditional and red-edge-based, to estimate various field-measured fire effects. Several fire effects were accurately estimated using a combination of red-edge and Burn Ratio indices and multivariate regression. These fire effects included post-fire dead PICO stumps, coarse wood percent cover, coarse wood volume, coarse wood mass, ash depth and percent cover of ghost logs. Of the indices generated, the most useful for estimating these fire effects were red-edge indices, especially those generated using Sentinel-2 band 5 (0.6955–0.7134 μm).

Despite the field data being of limited sample size and from a single forested ecosystem, this research shows that red-edge indices have potential for mapping various fire effects when used in combination. Further, although the methodology used to calculate the

indices and evaluate the comparisons is not novel, this study contributes to a growing body of literature, emphasizing the improved performance of red-edge-based indices over traditional near- and shortwave infrared-based indices. Future research should incorporate a larger validation data set and extend to other ecosystems, as these results are preliminary.

Author Contributions: Conceptualization, D.M.S., J.L.R.J., T.E.C. and D.R.B.; methodology, D.M.S.; validation, D.M.S.; formal analysis, D.M.S.; investigation, D.M.S., J.L.R.J., T.E.C. and D.R.B.; data curation, D.M.S.; writing—original draft preparation, D.M.S.; writing—review and editing, J.L.R.J., T.E.C. and D.R.B.; visualization, D.M.S. All authors have read and agreed to the published version of the manuscript.

Funding: This research received no external funding.

Data Availability Statement: The field data used in this study were collected by Turner et al. [17] and can be accessed at: <https://doi.org/10.6073/pasta/a1b7791376a04ce8c6ea9043547bb6af> (accessed on 12 May 2020). The other data used in this study (imagery, derived burn indices, etc.) are available upon request. Contact David M. Szpakowski (szpakowskid@mail.wou.edu) for access to these data.

Acknowledgments: We would like to thank Brian J. Harvey for connecting us to the field data used in this study.

Conflicts of Interest: The authors declare no conflict of interest.

References

1. Keeley, J.E. Fire Intensity, Fire Severity and Burn Severity: A Brief Review and Suggested Usage. *Int. J. Wildland Fire* **2009**, *18*, 116–126. [CrossRef]
2. Robichaud, P.R.; Lewis, S.A.; Laes, D.Y.M.; Hudak, A.T.; Kokaly, R.F.; Zamudio, J.A. Postfire Soil Burn Severity Mapping with Hyperspectral Image Unmixing. *Remote Sens. Environ.* **2007**, *108*, 467–480. [CrossRef]
3. Morgan, P.; Keane, R.E.; Dillon, G.K.; Jain, T.B.; Hudak, A.T.; Karau, E.C.; Sikkink, P.G.; Holden, Z.A.; Strand, E.K.; Morgan, P.; et al. Challenges of Assessing Fire and Burn Severity Using Field Measures, Remote Sensing and Modelling. *Int. J. Wildland Fire* **2014**, *23*, 1045–1060. [CrossRef]
4. Key, C.H.; Benson, N.C. Landscape Assessment (LA). In *FIREMON: Fire Effects Monitoring and Inventory System*; Lutes, D.C., Keane, R.E., Caratti, J.F., Key, C.H., Benson, N.C., Sutherland, S., Gangi, L.J., Eds.; Gen. Tech. Rep. RMRS-GTR-164-CD; U.S. Department of Agriculture, Forest Service, Rocky Mountain Research Station: Fort Collins, CO, USA, 2006; p. LA-1-55.
5. Epting, J.; Verbyla, D.; Sorbel, B. Evaluation of Remotely Sensed Indices for Assessing Burn Severity in Interior Alaska Using Landsat TM and ETM+. *Remote Sens. Environ.* **2005**, *96*, 328–339. [CrossRef]
6. Roy, D.P.; Boschetti, L.; Trigg, S.N. Remote Sensing of Fire Severity: Assessing the Performance of the Normalized Burn Ratio. *IEEE Geosci. Remote Sens. Lett.* **2006**, *3*, 112–116. [CrossRef]
7. Miller, J.D.; Thode, A.E. Quantifying Burn Severity in a Heterogeneous Landscape with a Relative Version of the Delta Normalized Burn Ratio (DNBR). *Remote Sens. Environ.* **2007**, *109*, 66–80. [CrossRef]
8. Parks, S.A.; Dillon, G.K.; Miller, C. A New Metric for Quantifying Burn Severity: The Relativized Burn Ratio. *Remote Sens.* **2014**, *6*, 1827–1844. [CrossRef]
9. *Earth Observation of Wildland Fires in Mediterranean Ecosystems*; Chuvieco, E. (Ed.) Springer: Berlin/Heidelberg, Germany, 2009; ISBN 978-3-642-01753-7.
10. Harris, S.; Veraverbeke, S.; Hook, S. Evaluating Spectral Indices for Assessing Fire Severity in Chaparral Ecosystems (Southern California) Using MODIS/ASTER (MASTER) Airborne Simulator Data. *Remote Sens.* **2011**, *3*, 2403–2419. [CrossRef]
11. Quintano, C.; Fernández-Manso, A.; Calvo, L.; Marcos, E.; Valbuena, L. Land Surface Temperature as Potential Indicator of Burn Severity in Forest Mediterranean Ecosystems. *Int. J. Appl. Earth Obs. Geoinf.* **2015**, *36*, 1–12. [CrossRef]
12. Gitas, I.; Mitri, G.; Veraverbeke, S.; Polychronaki, A. Advances in Remote Sensing of Post-Fire Vegetation Recovery—A Review. In *Remote Sensing of Biomass—Principles and Applications*; Fatoyinbo, L., Ed.; InTechOpen: London, UK, 2012; ISBN 978-953-51-0313-4.
13. Veraverbeke, S.; Hook, S.J. Evaluating Spectral Indices and Spectral Mixture Analysis for Assessing Fire Severity, Combustion Completeness and Carbon Emissions. *Int. J. Wildland Fire* **2013**, *22*, 707–720. [CrossRef]
14. Fernández-Manso, A.; Fernández-Manso, O.; Quintano, C. SENTINEL-2A Red-Edge Spectral Indices Suitability for Discriminating Burn Severity. *Int. J. Appl. Earth Obs. Geoinf.* **2016**, *50*, 170–175. [CrossRef]
15. Saberi, S.J. Quantifying Burn Severity in Forests of the Interior Pacific Northwest: From Field Measurements to Satellite Spectral Indices. M.S. Thesis, University of Washington, Seattle, Washington, USA, 2019.
16. Hudak, A.T.; Morgan, P.; Bobbitt, M.J.; Smith, A.M.S.; Lewis, S.A.; Lentile, L.B.; Robichaud, P.R.; Clark, J.T.; McKinley, R.A. The Relationship of Multispectral Satellite Imagery to Immediate Fire Effects. *Fire Ecol.* **2007**, *3*, 64–90. [CrossRef]
17. Turner, M.G.; Braziliunas, K.H.; Hansen, W.D.; Harvey, B.J. Plot-level field data and model simulation results, archived to accompany Turner et al. manuscript; reports data from summer 2017 sampling of short-interval fires that burned during summer

- 2016 in Greater Yellowstone. ver 2. Environmental Data Initiative. 2019. Available online: <https://portal.edirepository.org/nis/mapbrowse?packageid=edi.361.2> (accessed on 12 May 2020).
18. Turner, M.G.; Braziunas, K.H.; Hansen, W.D.; Harvey, B.J. Short-Interval Severe Fire Erodes the Resilience of Subalpine Lodgepole Pine Forests. *Proc. Natl. Acad. Sci. USA* **2019**, *116*, 11319–11328. [[CrossRef](#)]
 19. Gitelson, A.; Merzlyak, M.N. Spectral Reflectance Changes Associated with Autumn Senescence of *Aesculus Hippocastanum* L. and *Acer Platanoides* L. Leaves. Spectral Features and Relation to Chlorophyll Estimation. *J. Plant Physiol.* **1994**, *143*, 286–292. [[CrossRef](#)]
 20. Haaland, D.M.; Thomas, E.V. Partial Least-Squares Methods for Spectral Analyses. 2. Application to Simulated and Glass Spectral Data. *Anal. Chem.* **1988**, *60*, 1202–1208. [[CrossRef](#)]
 21. Navarro, G.; Caballero, I.; Silva, G.; Parra, P.-C.; Vázquez, Á.; Caldeira, R. Evaluation of Forest Fire on Madeira Island Using Sentinel-2A MSI Imagery. *Int. J. Appl. Earth Obs. Geoinf.* **2017**, *58*, 97–106. [[CrossRef](#)]
 22. Verbyla, D.; Lord, R. Estimating Post-fire Organic Soil Depth in the Alaskan Boreal Forest Using the Normalized Burn Ratio. *Int. J. Remote Sens.* **2008**, *29*, 3845–3853. [[CrossRef](#)]
 23. Lentile, L.B.; Smith, A.M.S.; Hudak, A.T.; Morgan, P.; Bobbitt, M.J.; Lewis, S.A.; Robichaud, P.R.; Lentile, L.B.; Smith, A.M.S.; Hudak, A.T.; et al. Remote Sensing for Prediction of 1-Year Post-Fire Ecosystem Condition. *Int. J. Wildland Fire* **2009**, *18*, 594–608. [[CrossRef](#)]
 24. García-Llamas, P.; Suárez-Seoane, S.; Fernández-Guisuraga, J.M.; Fernández-García, V.; Fernández-Manso, A.; Quintano, C.; Taboada, A.; Marcos, E.; Calvo, L. Evaluation and Comparison of Landsat 8, Sentinel-2 and Deimos-1 Remote Sensing Indices for Assessing Burn Severity in Mediterranean Fire-Prone Ecosystems. *Int. J. Appl. Earth Obs. Geoinf.* **2019**, *80*, 137–144. [[CrossRef](#)]
 25. Howe, A.A.; Parks, S.A.; Harvey, B.J.; Saberi, S.J.; Lutz, J.A.; Yocom, L.L. Comparing Sentinel-2 and Landsat 8 for Burn Severity Mapping in Western North America. *Remote Sens.* **2022**, *14*, 5249. [[CrossRef](#)]
 26. Chuvieco, E.; Riaño, D.; Danson, F.M.; Martin, P. Use of a Radiative Transfer Model to Simulate the Postfire Spectral Response to Burn Severity. *J. Geophys. Res. Biogeosci.* **2006**, *111*, G04S09. [[CrossRef](#)]
 27. Korets, M.A.; Ryzhkova, V.A.; Danilova, I.V.; Sukhinin, A.I.; Bartalev, S.A. Forest Disturbance Assessment Using Satellite Data of Moderate and Low Resolution. In *Environmental Change in Siberia: Earth Observation, Field Studies and Modelling*; Balzter, H., Ed.; Advances in Global Change Research; Springer: Dordrecht, The Netherlands, 2010; pp. 3–19. ISBN 978-90-481-8641-9.

Disclaimer/Publisher’s Note: The statements, opinions and data contained in all publications are solely those of the individual author(s) and contributor(s) and not of MDPI and/or the editor(s). MDPI and/or the editor(s) disclaim responsibility for any injury to people or property resulting from any ideas, methods, instructions or products referred to in the content.